Holographic antiferromagnetic quantum criticality and AdS$_2$ scaling limit

Rong-Gen Cai,[1,*] Run-Qiu Yang,[1,†] and F. V. Kusmartsev[2,‡]

[1]*State Key Laboratory of Theoretical Physics, Institute of Theoretical Physics,*
Chinese Academy of Sciences, Beijing 100190, China
[2]*Department of Physics, Loughborough University, Loughborough, Leicestershire,*
LE11 3TU, United Kingdom

A holographic description on the antiferromagnetic quantum phase transition (QPT) induced by the magnetic field and the criticality in the vicinity of the quantum critical point have been investigated numerically recently. In this paper, we show that the properties of QPT in this holographic model are governed by a CFT dual to the emergent AdS$_2$ in the IR region, which confirms that the dual boundary theory is a strong coupling theory with dynamic exponent $z = 2$ and logarithmic corrections appearing. We also compare them with the results from the Hertz model by solving the RG equation at its upper critical dimension and with some experimental data from pyrochlores $Er_{2-2x}Y_{2x}Ti_2O_7$ and $BiCoPO_5$.

I. INTRODUCTION

Quantum phase transitions (QPTs) happen at zero temperature. Such a phase transition and the critical behavior in the vicinity of the corresponding quantum critical points (QCPs) have attracted a great deal of interest both in theory and experiment recently [1–4]. In the phase diagram, a QCP separates an ordered phase from a disordered phase at zero temperature. In contrast to classical phase transition at $T > 0$ where thermal fluctuations play an important role, QPTs are induced by quantum fluctuations associated with the Heisenberg uncertainty and driven by a control parameter in the Hamiltonian rather than by temperature. Usually, the control parameter could be the composition, magnetic field, or pressure, etc. In condensed matter physics, such a quantum criticality is considered to be an important mechanism for some of the most interesting phenomena, especially in itinerant electronic systems [5,6] and other phenomenona involving strongly correlated many-body systems [7,8]. However, the complete theoretical descriptions valid at all the energy (or temperature) regions are still lacking.

One of the most interesting and intensively discussed QPTs is the ordered-disordered QPT in antiferromagnetic materials induced by magnetic field, such as $Cu_2(C_5H_12N_2)_2Cl_4$ [9], $KCuCl_3$ [10], $TlCuCl_3$ [11], $BiCoPO_5$ [12] and $Er_{2-2x}Y_{2x}Ti_2O_7$ [13]. A schematic phase diagram in the vicinity of a QPT as a function of the magnetic field is shown in Fig. 1, where we plot the Néel temperature $T_N(B)$ when $B < B_c$ and the spin gap $\Delta(B)$ at zero temperature when $B > B_c$. In the antiferromagnetic (AF) phase (ordered phase), the uniform spontaneously

staggered magnetization is accompanied by a long-ranged spin ordering, which persists up to a finite transition temperature T_N. When the magnetic field increases, the transition temperature T_N is suppressed. When the magnetic field arrives at its critical value, $B = B_c$, the transition temperature is suppressed to zero. When $B > B_c$ and $T = 0$, the quantum disordered (QD) phase has gapped magnetic excitations.

Another interesting feature in QPTs involving strong coupling is the so-called "hyperscaling violation" when the effective dimension is larger than or equal to d_c, the upper critical dimension of corresponding field theory. In general, for the case of dimensions less than d_c, in the vicinity of QCP, there are the hyperscaling relations for free energy density $F(b, T)$, Néel temperature T_N, correlation length ξ and characteristic energy Δ with respect to the tuning parameter $b = B/B_c - 1$ as follows,
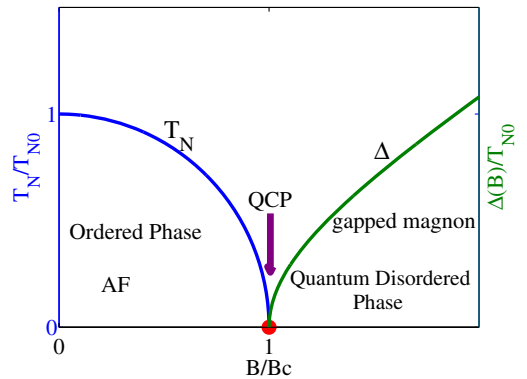

FIG. 1 (color online). Schematic phase diagram for a QPT, showing the Néel temperature and spin gap as functions of magnetic field [14]. For a magnetic QPT, the characteristic energy scales in the quantum disordered (QD) and AF phases are, respectively, the spin gap Δ and Néel temperature T_N, and both vanish at the QCP.

[*]cairg@itp.ac.cn
[†]aqiu@itp.ac.cn
[‡]F.Kusmartsev@lboro.ac.uk

$$F_c(b, T) = \lambda^{-(d+z)} F_c(b\lambda^{1/\nu}, T\lambda^z), \qquad b \to 0 \qquad (1a)$$

$$T_N \propto (-b)^\psi, \qquad b \to 0^-, \qquad (1b)$$

$$\xi \propto b^{-\nu}, \qquad \Delta \propto b^{z\nu} \quad b \to 0^+, \qquad (1c)$$

where d is the spatial dimension of the system, z is the dynamic exponent, and ψ and ν are two positive critical exponents depending on the model. $F_c(b, T)$ is the critical contribution to the free energy density defined by $F_c(b, T) = F(b, T) - F_{\text{reg}}(b, T)$, and λ is an arbitrary scale factor. The effective dimension of the system at QPT then is $d_{\text{eff}} = d + z$. The scaling relations (1c) are always valid. But the naive scaling relation (1a) is valid only when the effective dimension is less than the upper critical dimension, i.e., $d_{\text{eff}} < d_c$ [6]. In particular, when $d = z = 2$, the hyperscaling relations (1a) and (1b) are no longer valid. In that case, the quantum critical theory is not in a weak-coupling region in general. So for this case, a description of a strongly coupled effective field theory is called for near the QPTs [6].

In order to study and characterize strongly coupled quantum critical systems, some new methods are needed. The gauge/gravity duality or AdS/CFT correspondence provides us with a promising approach [15–18]. This duality relates a weak-coupling gravitational theory in a $(d + 1)$-dimensional asymptotically anti–de Sitter (AdS) space-time to a d-dimensional strong-coupling conformal field theory (CFT) in the AdS boundary. In recent years, this duality has been extensively applied in condensed matter systems. Some remarkable progress has been made in this direction, including holographic superfluids (superconductors) [19,20] (for a recent review, see [21]), (non-) Fermi liquids [22–24] and so on. The models in the AdS/CFT frame for ferromagnetism/paramagnetism and antiferromagnetism/paramagnetism phase transitions have also been proposed in [25,26]. Especially in Ref. [26], we found that the antiferromagnetic transition temperature T_N is indeed suppressed by an external magnetic field and tends to zero when the magnetic field approaches a critical value B_c. In this way we realized a holographic description of the antiferromagnetic quantum phase transition induced by an external magnetic field. Since the model involves rank-2 fields, the problems with ghost and causal violation may appear, which have not been discussed in that paper. Very recently, a modified model based on the previous works has been proposed in Ref. [27], which is shown to be ghost free and without causal violation but keeps all the significant results in the previous works qualitatively. For this modified model, a numerical investigation about the antiferromagnetic quantum phase transition induced by an external magnetic field was first presented in Ref. [28].

In this paper, we will further elaborate on the magnetic-induced QPT and study its critical behavior in some detail. In Sec. II, we will first review some basic properties of the holographic antiferromagnetic model by combining the ideas in Refs. [26,27] and studying the behavior of the Néel temperature T_N with respect to the external magnetic field, which shows that there is a critical magnetic field where quantum criticality appears and can be fitted well by adding a logarithmic correction to the usual power law form. In Sec. III, we will show that there is an emergent AdS$_2$ scaling limit which governs the low-frequency behaviors in the vicinity of QCP. By this emergent AdS$_2$ geometry, we confirm the numerical results in Sec. II and Ref. [28]. In Sec. IV, we give a dual field computation from the perturbation RG equation inspired by holographic results, which gives a confirmation of our holographic results. We will also discuss what our model can tell us about some real materials.

II. ANTIFERROMAGNETIC MODEL AND CRITICAL TEMPERATURE

The antiferromagnetic phase in materials is a magnetic ordered phase without net magnetization. For the simplest case, there are two different sublattices which have two spontaneous magnetic moments with the same magnitude but opposite direction. The order parameter then is the staggered magnetization, i.e., the difference between two different magnetic moments in two sublattices. Just as in the ferromagnetic phase, the time reversal transformation is also broken spontaneously in the antiferromagnetic phase.

A. Holographic antiferromagnetic model

In Ref. [25], we introduced an antisymmetric tensor field coupling with a U(1) strength field to describe the phase which has one uniform spontaneous magnetization. In order to describe a spontaneous magnetic ordered phase which has a staggered magnetization, we introduce two antisymmetric tensor fields. Following Ref. [26] and Ref. [27], the action we will consider here takes the form

$$S = \frac{1}{2\kappa^2} \int d^4x \sqrt{-g} \left[R + \frac{6}{L^2} - F^{\mu\nu}F_{\mu\nu} \right.$$
$$\left. - \lambda^2 (L_1 + L_2 + L_{12}) \right], \qquad (2)$$

where

$$L_{12} = \frac{k}{2} M^{(1)\mu\nu} M^{(2)}_{\mu\nu},$$

$$L_{(a)} = \frac{1}{12}(dM^{(a)})^{\mu\nu\tau}(dM^{(a)})_{\mu\nu\tau} + \frac{m^2}{4} M^{(a)\mu\nu} M^{(a)}_{\mu\nu}$$
$$+ \frac{1}{2} M^{(a)\mu\nu} F_{\mu\nu} + J V(M^{(a)}_{\mu\nu}),$$

$$V(M^{(a)}_{\mu\nu}) = (^*M^{(a)}_{\mu\nu} M^{(a)\mu\nu})^2,$$

$$a = 1, 2. \qquad (3)$$

L is the radius of AdS space, and $2\kappa^2 = 16\pi G$ with G the Newton constant. $*$ is the Hodge star dual operator. In this model, k, m^2 and J are all model parameters with $J < 0$. λ^2 characterizes the backreaction of the two polarization fields $M_{\mu\nu}^{(a)}$ with $a = 1, 2$ to the background geometry,[1] and L_{12} describes the interaction between two polarization fields. The equations of motion for polarization fields read

$$3\nabla^\tau\nabla_{[\tau}M_{\mu\nu]}^{(a)} - m^2 M_{\mu\nu}^{(a)} - kM_{\mu\nu}^{(b)} - JV'(a)_{\mu\nu} - F_{\mu\nu} = 0.$$

(4)

Here $(a, b) = (1, 2)$ or $(2, 1)$ and $V'(a)_{\mu\nu} = (*M^{(a)}{}_{\tau\sigma}M^{(a)\tau\sigma}) *M^{(a)}{}_{\mu\nu}$. In the probe limit of $\lambda \to 0$, we can neglect the backreaction of the two polarization fields on the background geometry. The background we will consider is a dyonic Reissner-Nordström-AdS black brane solution of the Einstein-Maxwell theory with a negative cosmological constant, and the metric reads [29]

$$ds^2 = r^2(-f(r)dt^2 + dx^2 + dy^2) + \frac{dr^2}{r^2 f(r)},$$

$$f(r) = 1 - \frac{1 + \mu^2 + B^2}{r^3} + \frac{\mu^2 + B^2}{r^4}.$$

(5)

Here both the black brane horizon and AdS radius have been set to unity. The temperature of the black brane is

$$T = \frac{1}{4\pi}(3 - \mu^2 - B^2).$$

(6)

For the solution (5), the corresponding gauge potential is $A_\mu = \mu(1 - 1/r)dt + Bxdy$. Here μ is the chemical potential and B can be viewed as the external magnetic field in the dual boundary field theory. The zero-temperature limit then corresponds to $B^2 + \mu^2 = 3$.

In order to describe the antiferromagnetic phase transition, following Ref. [26], we consider $M_{\mathrm{tr}}^{(a)}, M_{xy}^{(a)}$ $(a = 1, 2)$ and define

$$\alpha = \frac{1}{2}(M_{xy}^{(1)} + M_{xy}^{(2)}), \qquad \beta = \frac{1}{2}(M_{xy}^{(1)} - M_{xy}^{(2)}),$$

$$p_1 = \frac{1}{2}(M_{\mathrm{tr}}^{(1)} + M_{\mathrm{tr}}^{(2)}), \qquad p_2 = \frac{1}{2}(M_{\mathrm{tr}}^{(1)} - M_{\mathrm{tr}}^{(2)}).$$

(7)

Then different values of α and β correspond to different magnetic phases. The staggered magnetization $N^\dagger$ and total magnetization N can be defined as

---

[1]By rescaling the tensor fields $M^{(a)}$ and the parameter J, the parameter λ^2 can also be interpreted as the coupling strength between the tensor fields and background Maxwell field strength.

$$N^\dagger/\lambda^2 = -\int_1^\infty \frac{\beta}{r^2}\,dr,$$

$$N/\lambda^2 = -\int_1^\infty \frac{\alpha}{r^2}\,dr.$$

(8)

When the external magnetic field $B = 0$, the antiferromagnetic phase corresponds to the phase with nonzero staggered magnetization but zero total magnetization density.

We put the expressions (7) into Eq. (4), and we have the equations for α and β as

$$\alpha'' + \frac{f'\alpha'}{f} - \left[\frac{4J(p_1^2 + p_2^2)}{r^2 f} + \frac{m^2 + k}{r^2 f}\right]\alpha + \frac{8Jp_1 p_2 \beta}{r^2 f}$$
$$+ \frac{B}{r^2 f} = 0,$$

$$\beta'' + \frac{f'\beta'}{f} - \left[\frac{4J(p_1^2 + p_2^2)}{r^2 f} + \frac{m^2 - k}{r^2 f}\right]\beta + \frac{8Jp_1 p_2 \alpha}{r^2 f} = 0,$$

(9)

with

$$p_1 = \frac{r^2[(m^2 - k)r^4 - 4J(\alpha^2 + \beta^2)]\mu}{16J^2(\alpha^2 - \beta^2)^2 - 8J(\alpha^2 + \beta^2)m^2 r^4 + (m^4 - k^2)r^8},$$

$$p_2 = \frac{8J\mu\alpha\beta r^2}{16J^2(\alpha^2 - \beta^2)^2 - 8J(\alpha^2 + \beta^2)m^2 r^4 + (m^4 - k^2)r^8}.$$

(10)

The behavior of the solutions of Eqs. (9) in the UV region (near the AdS boundary) depends on the value of $m^2 + k$. When $m^2 + k = 0$, the asymptotic solutions will have a logarithmic term, but we will not consider this case in the present paper. On the other hand, when $m^2 + k \neq 0$, we have the asymptotic solution,

$$\alpha_{UV} = \alpha_+^{UV} r^{(1+\delta_1)/2} + \alpha_-^{UV} r^{(1-\delta_1)/2} - \frac{B}{m^2 + k},$$

$$\beta_{UV} = \beta_+^{UV} r^{(1+\delta_2)/2} + \beta_-^{UV} r^{(1-\delta_2)/2},$$

$$\delta_1 = \sqrt{1 + 4k + 4m^2}, \qquad \delta_2 = \sqrt{1 - 4k + 4m^2},$$

(11)

where $\alpha_\pm^{UV}$ and $\beta_\pm^{UV}$ are all finite constants. We require that the condensation happens spontaneously when $B = 0$. By the inspirit of AdS/CFT, we impose the following boundary conditions:

$$\alpha_+^{UV} = \beta_+^{UV} = 0.$$

(12)

B. Conditions for antiferromagnetic phase transition when B = 0

In our model, there are three parameters J, m^2 and k. In order that the dual boundary theory can describe an

antiferromagnetic system, these parameters need to satisfy some conditions.

First, from the asymptotic behaviors in Eqs. (11), we see that the BF bound requires that m^2 and k satisfy $1 + 4m^2 > 4|k|$. On the other hand, because of $J < 0$, in order to make p_1 and p_2 finite in the region (r_h, ∞), we need the following conditions:

$$m^2 > |k| \Leftrightarrow \delta_1 > 1, \quad \text{and} \quad \delta_2 > 1. \qquad (13)$$

If conditions (13) are broken, we can see that the components p_1, p_2 will diverge somewhere, which leads that there is some point where the energy-momentum tensor associated with these tensor fields diverges. So in this case, the bulk geometry becomes unstable and the probe limit is broken.

We can explain the conditions (12) and (13) in another way. By the definitions (7), we see that the terms of $\alpha_{\pm}^{UV}, \beta_{\pm}^{UV}$ and B all appear in the asymptotic solutions of $M_{xy}^{(1)}$ and $M_{xy}^{(1)}$. Since we need the system to be dominated by an external magnetic field when $B \neq 0$, so the magnetic term should be the leading term near the boundary. This can be reached only when both the boundary conditions (12) and (13) are satisfied.

Second, as pointed out in Ref. [26], in order to get an antiferromagnetic phase transition below a critical temperature when $B = 0$, we need β to condense spontaneously, but α cannot; in other words, the system is stable for α but not for β. In the RN-AdS black brane background, this can be achieved if the AdS$_2$ BF bound is satisfied for α but violated for β near the horizon when $T = 0$. As in the critical cases for instability, we can treat α and β as small quantities, so we get linearized equations for them,

$$\alpha'' + \frac{f'\alpha'}{f} - \left[\frac{4Jp_1^2}{r^2 f} + \frac{m^2 + k}{r^2 f}\right]\alpha = 0,$$

$$\beta'' + \frac{f'\beta'}{f} - \left[\frac{4Jp_1^2}{r^2 f} + \frac{m^2 - k}{r^2 f}\right]\beta = 0, \qquad (14)$$

with $p_1 = \mu/[(m^2 + k)r^2]$. Then the zero temperature corresponds to $\mu = \sqrt{3}$. Let $r_* = 1/(r - 1)$, when $r_* \to \infty$; namely, near the horizon, we have the following asymptotic solutions for α and β:

$$\alpha_{\text{IR}} = \alpha_+^{\text{IR}} r_*^{-(1+\delta_1^*)/2} + \alpha_-^{\text{IR}} r_*^{-(1-\delta_1^*)/2},$$

$$\beta_{\text{IR}} = \beta_+^{\text{IR}} r_*^{-(1+\delta_2^*)/2} + \beta_-^{\text{IR}} r_*^{-(1-\delta_2^*)/2},$$

$$\delta_1^* = \sqrt{1 + 2(k + m^2 + 4Jp_{10}^2)/3},$$

$$\delta_2^* = \sqrt{1 + 2(m^2 - k + 4Jp_{10}^2)/3}. \qquad (15)$$

Here $p_{10} = \sqrt{3}/(m^2 + k)$, and $\alpha_{\pm}^{\text{IR}}$ and $\beta_{\pm}^{\text{IR}}$ are all finite constants. As a result, to have the antiferromagnetic
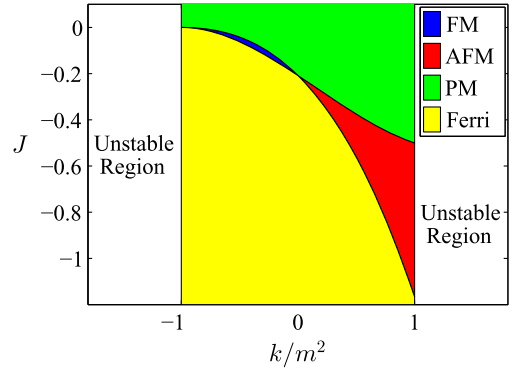

FIG. 2 (color online). Zero-temperature phase diagram obtained in the plane of the holographic model parameters, J and k/m^2. It was calculated when $B = 0$ and $m^2 = 1$. Here FM, AFM, PM and Ferri stand for ferromagnetic, antiferromagnetic, paramagnetic and ferrimagnetic phases, respectively.

instability requires that the parameters satisfy the following conditions:

$$\begin{cases} 1 + 2(k + m^2 + 4Jp_{10}^2)/3 > 0, \\ 1 + 2(m^2 - k + 4Jp_{10}^2)/3 < 0, \end{cases} \qquad (16)$$

which lead to the following constraint,

$$J_c^+(k, m^2) < J < J_c^-(k, m^2), \quad \text{and} \quad k > 0, \qquad (17)$$

with $J_c^{\pm}(k, m^2) = -(m^2 + k)^2(m^2 + 3/2 \pm k)/12$.

When the external magnetic field $B = 0$, for given mass square m^2, the zero-temperature phase of the dual boundary then depends on the parameters J and k. A typical example for $m^2 = 1$ is plotted in Fig. 2. The red region corresponds to the case that parameters satisfy the conditions (13) and (17), which is what we will consider in this paper.

C. Néel temperature and quantum criticality

When the magnetic field is absent, i.e., $B = 0$, under the conditions (12), (13) and (17), the solution of α is always zero, which means there does not exist spontaneous magnetization. But there is a critical temperature T_{N0}, lower than which a nonvanishing β begins to appear, which shows the system transits into the antiferromagnetic phase and gives a nonzero spontaneous staggered magnetization.

On the other hand, if we turn on an external magnetic field B, we have $\alpha \neq 0$. When the external magnetic field is small, the value of $|\alpha|$ will increase with the increasing of B. Since the equation for β couples with α, the staggered magnetization is also influenced by the magnetic field. This influence can be seen clearly from the effective mass square of β in the IR region, namely, the near horizon region. Near the horizon, we have

$$m^2_{\beta\text{eff}}\big|_{r_h} = \frac{4J\mu^2}{(k+m^2)^2} + m^2 - k + \frac{64J^2\mu^2\alpha^2}{(k+m^2)^2(m^2-k)}.$$

(18)

Under the restriction (13), we can see that, for the small magnetic field, the effective mass square of β in the IR region will increase with the magnetic field B, which leads the nonzero solution of β to appear in lower and lower temperatures with an increasing magnetic field. Thus, the antiferromagnetic critical temperature T_N will be suppressed by the external magnetic field.

When the external magnetic field is not very small, because of the nonlinear coupling between β and α, it is not easy to directly give the relation between the effective mass square of β and the external magnetic field. Instead, the behavior of T_N with respect to the magnetic field can be found numerically. Near the critical temperature, the staggered magnetization is very small; i.e., β is a small quantity. In that case we can neglect the nonlinear terms of β in Eqs. (9), which leads to

$$\alpha'' + \frac{f'\alpha'}{f} - \frac{m^2_{\alpha\text{eff}}}{r^2 f}\alpha = \frac{B}{r^2 f},$$

$$\beta'' + \frac{f'\beta'}{f} - \frac{m^2_{\beta\text{eff}}}{r^2 f}\beta = 0,$$

(19)

with

$$m^2_{\alpha\text{eff}} = 4Jp_1^2 + m^2 + k,$$

$$m^2_{\beta\text{eff}} = m^2 - k + 4Jp_1^2 + 8Jp_1\tilde{p}_2\alpha^2,$$

$$p_1 = \frac{r^2\sqrt{3 - B^2 - 4\pi T}}{(m^2+k)r^4 - 4J\alpha^2},$$

$$\tilde{p}_2 = \frac{8Jr^2\sqrt{3 - B^2 - 4\pi T}}{(4J\alpha^2 - m^2 r^4)^2 - k^2 r^8}.$$

(20)

When $T \neq 0$, in the IR region, the regularity of the solution gives the following initial conditions,

$$\begin{cases} \alpha' = \frac{\alpha m^2_{\alpha\text{eff}} + B}{4\pi T}, \\ \beta' = \frac{\beta m^2_{\beta\text{eff}}}{4\pi T}, \end{cases}$$

(21)

at the horizon. Without loss of generality, we can set $\beta(r_h) = 1$ due to the linearity of the equation of β.

When $T_N = 0$, the initial conditions (21) imply that

$$B = -\alpha m^2_{\alpha\text{eff}}\big|_{r_h}, \quad \text{and} \quad m^2_{\beta\text{eff}}\big|_{r_h} = 0$$

(22)

at the horizon. For given parameters J, m^2 and k, these two equations give the solution $\alpha(r_h) = \alpha_c$ and $B = B_c$. Here α_c is the initial value of α at the IR fixed point, and B_c is the critical magnetic field where the QPT occurs.

In Fig. 3, we plot the Néel temperature T_N in the case of $B < B_c$. Because different parameters satisfying restrictions (13) and (17) give qualitatively the same results, we here just show a typical example by taking $m^2 = 1, k = 7/8$ and $J = -2/3$. Increasing the magnetic field from zero to B_c, the Néel temperature decreases from T_{N0} to zero. For small B, numerical results show that $T_N - T_{N0} \propto B^2$. When the magnetic field approaches B_c, we find that the Néel temperature is fitted well by the following relation:

$$\tilde{T}_N / \ln \tilde{T}_N \simeq -0.4074(1 - B/B_c).$$

(23)

Here $\tilde{T}_N = T_N/T_{N0}$ and T_{N0} is the Néel temperature in the case of $B = 0$.

The numerical results shown in Fig. 3 and the relation (23) show that there is indeed a critical magnetic field B_c at which the critical temperature for staggered magnetization, i.e. β, is zero. So a quantum phase transition occurs, which separates the antiferromagnetic phase and a quantum disordered phase at zero temperature. We can also obtain other critical properties in the vicinity of QCP by numerical methods [28]. In particular, in the vicinity of QCP, this model gives a dispersion relation for quasiparticles such as $\omega \sim q^2$ with energy ω and moment q, which shows that the boundary critical theory is a strong coupling theory with dynamic exponent $z = 2$ [6]. This agrees with the results from condensed matter theory about antiferromagnetic metal [6] and from the holographic model proposed in Ref. [30].

The behavior of the Néel temperature in the vicinity of QCP is quite nontrivial and needs to be further understood. The relation (23) is not the usual power-law behavior in (1b) or the square-root form. However, it agrees with the predication in the two-dimension QPTs in the strong-coupling case [2,6,31]. The $d = z = 2$ quantum critical
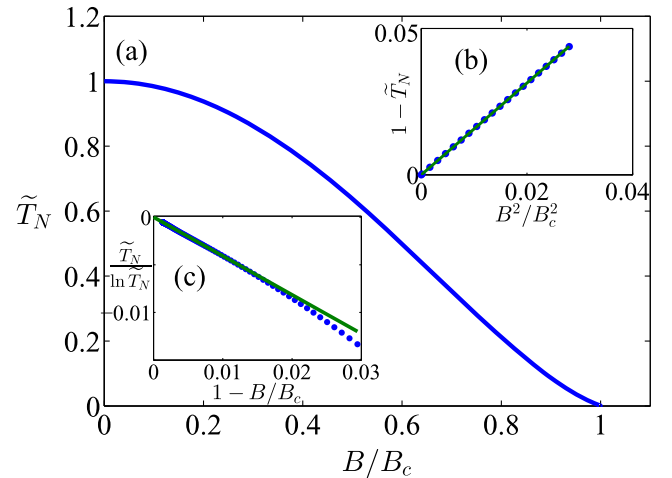

FIG. 3 (color online). The antiferromagnetic critical temperature T_N versus the magnetic field B. (a) In the whole region of $0 \leq B \leq Bc$. (b) In the region of $B \ll B_c$. (c) In the region of $1 - B/B_c \to 0^+$.

theory is in general not in a weak coupling region for any $T > 0$ and a strongly coupled effective classical model emerges that can be used to determine the critical dynamics [32]. As pointed out in Ref. [28], it is the reason why the AdS/CFT correspondence is very suitable for this description. In addition, the original numerical results in Ref. [28] need to be confirmed, especially for the logarithmic correction scaling relation Eq. (23). And we also need some more careful investigation to provide insight into physical properties in the vicinity of QCP in this holographic model. The most important is to clarify the relationship between this holographic model and the traditional theories of QPT and to know what we can learn about the real materials in the experiment from our holographic results. These are our goals in the following sections.

III. EMERGENT IR GEOMETRY AND THE BEHAVIORS NEAR QCP

In order to understand the scaling relation (23) and other numerical results presented in Ref. [28], we now pay attention to the background geometry in the zero-temperature case. As the similar situation in Ref. [33], we will see that our numerical results about the behaviors in the vicinity of QCP are just controlled by the IR geometry which is just the emergent AdS_2 geometry.

A. IR fixed point and critical magnetic field

In the vicinity of QCP, the system is dominated by the features of the IR region, where an AdS_2 geometry emerges. Following Ref. [33], we introduce a new length scale $\tilde{r}$,

$$\mu^2 + B^2 = 3\tilde{r}^4. \tag{24}$$

Then the temperature of the black brane background can be written as

$$T = \frac{3}{4\pi}(1 - \tilde{r}^4). \tag{25}$$

Using this new scale, we define a new radial coordinate ξ and time τ as

$$r - \tilde{r} = \frac{\lambda}{6\xi}, \qquad 1 - \tilde{r} = \frac{\lambda}{6\xi_0}, \qquad t = \lambda^{-1}\tau, \qquad \lambda \to 0. \tag{26}$$

Using the variable ξ, we can define an inner IR boundary at $\xi \to \xi_0$ and an outer IR boundary at $\xi \to 0^+$ (see Fig. 4). The line element can be written as

$$ds^2 = \frac{1}{6\xi^2}\left[-\left(1 - \frac{\xi^2}{\xi_0^2}\right)d\tau^2 + \left(1 - \frac{\xi^2}{\xi_0^2}\right)^{-1}d\xi^2\right] + (dx^2 + dy^2). \tag{27}$$
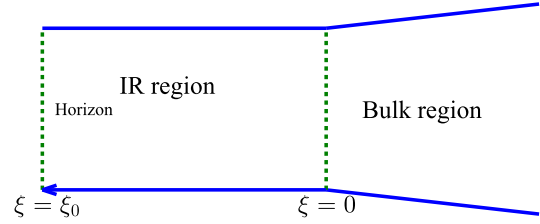

FIG. 4 (color online). A schematic figure for the inner IR region and outer bulk region. The horizon is located at $\xi = \xi_0$. The near horizon region is $\xi_0 < \xi < 0$, where an AdS_2 geometry emerges. The bulk region is not covered by the ξ coordinate. The solutions in the IR region and in the bulk region should be matched at $\xi = 0$.

Then the radial function $f(r)$ is

$$f(\xi) = \frac{\lambda^2}{6\xi^2}\left(1 - \frac{\xi^2}{\xi_0^2}\right). \tag{28}$$

The temperature with respect to τ is

$$\tilde{T} = \lambda^{-1}T = \frac{1}{2\pi\xi_0}. \tag{29}$$

Here the case of zero temperature corresponds to an infinity ξ_0. Note that in the scaling limit (26), finite τ corresponds to the long time limit of the original time coordinate. Thus, in the language of the boundary field theory, the solution (27) corresponds to the low-frequency limit.

Since the radial coordinate can be considered as the resolution scale for the dual theory, the evolution of the geometry and the fields propagating therein along this radial direction represent the RG flow of the dual field theory. Using the coordinate transformations (26), we can rewrite Eqs. (9) in the limit of $\lambda \to 0$ as

$$\frac{d^2\alpha}{d\xi^2} - \frac{2\xi}{\xi_0^2 - \xi^2}\frac{d\alpha}{d\xi} - \frac{\xi_0^2(B + \alpha m_{\alpha\text{eff}}^2)}{6\xi^2(\xi_0^2 - \xi^2)} = 0,$$

$$\frac{d^2\beta}{d\xi^2} - \frac{2\xi}{\xi_0^2 - \xi^2}\frac{d\beta}{d\xi} - \frac{\xi_0^2 m_{\beta\text{eff}}^2\beta}{6\xi^2(\xi_0^2 - \xi^2)} = 0. \tag{30}$$

In the zero-temperature case, which corresponds to $\xi_0 \to \infty$, Eqs. (30) become

$$\frac{d^2\alpha}{d\xi^2} - \frac{B + m_{\alpha\text{eff}}^2\alpha}{6\xi^2} = 0,$$

$$\frac{d^2\beta}{d\xi^2} - \frac{m_{\beta\text{eff}}^2}{6\xi^2}\beta = 0. \tag{31}$$

With the boundary conditions that α and β are both finite at inner IR boundary and outer IR boundary or the existence of IR fixed points for α and β in the IR region, these two equations have regular solutions only when α and β are both constants. As a result, we have,

$$B + m_{\alpha\text{eff}}^2 \alpha = 0, \qquad m_{\beta\text{eff}}^2 = 0. \qquad (32)$$

This is just what we have obtained in Eqs. (22). Note that in that case, α, β, p_1 and $\tilde{p}_2$ are all constants in the IR region, and so $\alpha m_{\alpha\text{eff}}^2$ and $m_{\beta\text{eff}}^2$ are also constants in the IR region. With the restrictions that $m^2 \geq |k|$ and J satisfy Eqs. (17), we can conclude that when $B < B_c$, the solution with $\beta \neq 0$ exists. But when $B > B_c$, there is only a trivial solution with $\beta = 0$, by matching into the bulk region, which will give a trivial solution such that $\beta(r) = 0$ in the whole bulk region. Thus, there is a phase transition at $B = B_c$ at zero temperature, which divides an AFM phase from a quantum disordered phase.

B. Linear perturbations and dynamic exponent

In order to compute the magnetic fluctuations in the vicinity of QCP, we turn on the perturbations of two polarization fields. Because of the nonlinear term in Eqs. (4), all the components couple with each other. As a result, we need to consider the perturbations for all the components, i.e.,

$$\delta M_{\mu\nu}^{(a)} = \epsilon C_{\mu\nu}^{(a)} e^{-i(\omega t + qx)}, \qquad (\mu, \nu) \neq (r, y), (t, x)$$
$$\delta M_{\mu\nu}^{(a)} = i\epsilon C_{\mu\nu}^{(a)} e^{-i(\omega t + qx)}, \qquad (\mu, \nu) = (r, y), (t, x). \qquad (33)$$

Substituting the ansatz (33) into (4) and computing up to the linear order of ϵ, we can get the equations for perturbations. When $\omega, q \neq 0$, however, we cannot decouple all the equations. In general, therefore, we need to solve the 6×2 components together in order to determine the dispersion relation. But if we consider the behavior for low frequency and small wave vector in the vicinity of QCP, i.e., $\omega \to 0$ and $q \to 0$, the problem can be simplified. In that case, the equations for $C_{tx}^{(a)}$ and $C_{ry}^{(a)}$ decouple from the others and can be neglected. Then we obtain the 4×2 coupled equations,

$$[(q^2 + m^2)r^2 - 4JM_{xy}^{(a)2}]C_{\text{tr}}^{(a)} + q^2 C_{rx}^{(a)} - 8JM_{xy}^{(a)} M_{\text{tr}}^{(a)} C_{xy}^{(a)} + kr^2 C_{\text{tr}}^{(b)} = 0,$$

$$\left(m^2 - \frac{\omega^2}{r^2 f}\right) C_{rx}^{(a)} + \frac{4JC_{ty}^{(a)} M_{xy}^{(a)} M_{\text{tr}}^{(a)}}{r^4 f} + kC_{rx}^{(b)} = 0,$$

$$C_{ty}^{(a)\prime\prime} - \frac{m^2 C_{ty}^{(a)}}{r^2 f} - \frac{kC_{ty}^{(b)}}{r^2 f} + \frac{4JC_{rx}^{(a)} M_{xy}^{(a)} M_{\text{tr}}^{(a)}}{r^4 f} = 0,$$

$$C_{xy}^{(a)\prime\prime} + \frac{f' C_{xy}^{(a)\prime}}{f} + \left(\frac{\omega^2}{r^2 f^2} - \frac{m^2 + 4JM_{\text{tr}}^{(a)2}}{r^2 f}\right) C_{xy}^{(a)\prime} - \frac{C_{ty}^{(a)} q\omega}{r^4 f^2} - \frac{kC_{xy}^{(b)}}{r^2 f} - \frac{8JC_{\text{tr}}^{(a)} M_{xy}^{(a)} M_{\text{tr}}^{(a)}}{r^2 f} = 0, \qquad (34)$$

with $(a, b) = (1, 2)$ or $(2, 1)$. In the paramagnetic phase, i.e., $M_{xy}^{(1)} = M_{xy}^{(2)}$ and $M_{\text{tr}}^{(1)} = M_{\text{tr}}^{(2)}$, the second and the third equations in (34) show that $C_{ty}^{(1)} = C_{ty}^{(2)}$ and $C_{rx}^{(1)} = C_{rx}^{(2)}$. Let $\tilde{\beta} = (C_{xy}^{(1)} - C_{xy}^{(2)})/2$, then we obtain,

$$\tilde{\beta}'' + \frac{f'\tilde{\beta}'}{f} + \left[\frac{\omega^2 - Qq^2 f}{r^2 f^2} - \frac{m_{\beta\text{eff}}^2}{r^2 f}\right] \tilde{\beta} + \mathcal{O}(q^4) = 0, \qquad (35)$$

with

$$Q = \frac{64J^2\alpha^2 p_1^2}{[(m^2 - k^2)r^4 - 4J\alpha^2]^2} > 0. \qquad (36)$$

As q is infinitesimal, we can neglect the high-order term $\mathcal{O}(q^4)$. Note that no matter how small ω and q are, we here cannot neglect the $(\omega^2 - Qq^2 f)/(r^2 f^2)$ term, because it diverges when $f = 0$.

In order to analyze the antiferromagnetic dispersion relation near the QCP for small frequency ω and wave vector q, we can take the IR-UV matching method proposed in Ref. [33]. We first compute the retarded Green's function in the IR region. Using the metric (27) in the limit of $\xi_0 \to \infty$ and the scale frequency as $\tilde{\omega} = \lambda\omega$, we obtain

$$\frac{d^2\tilde{\beta}}{d\xi^2} + (\tilde{\omega}^2 - Q_0 q^2/6\xi^2)\tilde{\beta} = 0, \qquad (37)$$

where we have used the results (32). Q_0 is the value of Q in the IR region. Because α is a constant in the IR region, Q is also a constant in the IR region. Solving this equation with the ingoing condition at $\xi \to \infty$, we have

$$\tilde{\beta} \propto \sqrt{\xi} H_\nu^{(1)}(\tilde{\omega}\xi). \qquad (38)$$

Here $H_\nu^{(1)}(x)$ is the first Hankel function with order $\nu = \sqrt{9 + 6Q_0 q^2}/6$. Using the properties of the Hankel function and the fact that $q \ll 1$, we can find that the asymptotic solution for β in the outer IR region is

$$\tilde{\beta} \propto \xi^{-Q_0 q^2/2} + \mathcal{G}(\tilde{\omega})\xi^{1 + Q_0 q^2/2}, \qquad (39)$$

with the IR retarded Green's function $\mathcal{G}(\tilde{\omega}) \propto \tilde{\omega}^{Q_0 q^2/3}$. Then using the method in Ref. [33], one can find that the retarded Green's function can be expanded in small ω as

$$G(\omega) \propto \frac{b_+^{(0)} + \omega b_+^{(1)} + O(\omega^2) + \mathcal{G}(\omega)(b_-^{(0)} + \omega b_-^{(1)} + O(\omega^2))}{a_+^{(0)} + \omega a_+^{(1)} + O(\omega^2) + \mathcal{G}(\omega)(a_-^{(0)} + \omega a_-^{(1)} + O(\omega^2))},$$

(40)

with $b_\pm^{(i)}$ and $a_\pm^{(i)}$ the analytical functions of q^2. By neglecting the irrelevant parts in (40), the retarded Green's function can be written as the following form for small ω and q,

$$G(\omega) = \frac{Z}{-q^2 + a_1 \omega + a_2 \omega^{Q_0 q^2/3}},$$

(41)

with some constant Z. Considering the fact that when $q = 0$, the retarded Green's function has a pole at $\omega = 0$, and we have $a_2 = 0$. Then the dispersion relation is determined by the equation

$$-q^2 + a_1 \omega = 0,$$

(42)

which tells us $\omega \sim q^2$. Thus, we obtain the dynamic exponent $z = 2$.

One should note that, in general, the coefficients appearing in (40) have scaling dimensions, and so do those for a_1 in (42). From the expression (42), we find that a_1 has scaling dimension 1. Thus, under the scaling transformation such that $r \to \lambda r$, $(t, x, y) \to \lambda^{-1}(t, x, y)$, which induces the transformations such that $\omega \to \lambda \omega$, $q \to \lambda q$ and $a_1 \to \lambda a_1$, Eq. (42) is invariant. As a result, the dynamic exponent $z = 2$ is compatible with scaling symmetry.

C. The scaling relation of T_N with B near the QCP

Now let us find the scaling relation of T_N with B in the region of $B \to B_c^-$. The method we will take is similar to the one as in the previous subsection. We first compute the Green's function at finite temperature in the IR region, and then match it with the bulk solution.

In the IR region, near the fixed point $B = B_c + \delta B$ with $\delta B \to 0^-$, we can neglect the nonlinear term of β and can get the equations with finite ξ_0,

$$\frac{d^2\alpha}{d\xi^2} - \frac{2\xi}{\xi_0^2 - \xi^2}\frac{d\alpha}{d\xi} = \frac{\xi_0^2[B + m_{\alpha\text{eff}}^2\alpha]}{6\xi^2(\xi_0^2 - \xi^2)},$$

$$\frac{d^2\beta}{d\xi^2} - \frac{2\xi}{\xi_0^2 - \xi^2}\frac{d\beta}{d\xi} = \frac{\xi_0^2 m_{\beta\text{eff}}^2 \beta}{6\xi^2(\xi_0^2 - \xi^2)}.$$

(43)

Under the boundary conditions that α and β are both finite at $\xi = 0$ and ξ_0, the solutions for Eqs. (43) are constants. Then we have the solution such that

$$B_c + \delta B + m_{\alpha\text{eff}}^2\alpha = 0, \qquad \beta = 0, \qquad (44)$$

Using Eqs. (22), up to the order of δB, we find that Eqs. (44) give the solution $\alpha = \alpha_0 \equiv \alpha_c + \delta\alpha$ with

$$\delta\alpha = -\frac{\delta B}{(m_{\alpha\text{eff}}^2 + \partial m_{\alpha\text{eff}}^2/\partial\alpha)}\bigg|_{\alpha=\alpha_c}.$$

(45)

In order to compute the retarded Green's function, we consider the deviations from the fixed point with $\beta = 0 + \beta_1$ and $\alpha = \alpha_0 + \alpha_1$. Note that in $\delta B \to 0^-$, up to the linear order of β_1 and α_1, we have the equations of the fluctuations

$$\frac{d^2\alpha_1}{d\xi^2} - \frac{2\xi}{\xi_0^2 - \xi^2}\frac{d\alpha_1}{d\xi} = \frac{\xi_0^2(m_{\alpha\text{eff}}^2 + \partial m_{\alpha\text{eff}}^2/\partial\alpha)\alpha_1}{6\xi^2(\xi_0^2 - \xi^2)},$$

$$\frac{d^2\beta_1}{d\xi^2} - \frac{2\xi}{\xi_0^2 - \xi^2}\frac{d\beta_1}{d\xi} = \frac{\partial m_{\beta\text{eff}}^2}{\partial\alpha}\frac{\delta\alpha\beta_1}{6\xi^2(\xi_0^2 - \xi^2)}.$$

(46)

Here the effective mass terms and their derivatives are taken from the value at $\alpha = \alpha_0$. The solutions for α_1 and β_1 can be expressed as hypergeometric functions as

$$\alpha_1 = \sum_\pm \left(\frac{\xi}{\xi_0}\right)^{\frac{1\pm\delta_\alpha}{2}} C_\pm^{(\alpha)} {}_2F_1\left[\frac{3\pm\delta_\alpha}{4}, \frac{1\pm\delta_\alpha}{4}; 1\pm\frac{\delta_\alpha}{2}; \frac{\xi}{\xi_0}\right],$$

$$\beta_1 = \sum_\pm \left(\frac{\xi}{\xi_0}\right)^{\frac{1\pm\delta_\beta}{2}} C_\pm^{(\beta)} {}_2F_1\left[\frac{3\pm\delta_\beta}{4}, \frac{1\pm\delta_\beta}{4}; 1\pm\frac{\delta_\beta}{2}; \frac{\xi}{\xi_0}\right]$$

(47)

with $\delta_\alpha = \sqrt{1 + 2(m_{\alpha\text{eff}}^2 + \partial m_{\alpha\text{eff}}^2/\partial\alpha)/3}$ and $\delta_\beta = \sqrt{1 + \frac{2}{3}(\partial m_{\beta\text{eff}}^2/\partial\alpha)\delta\alpha}$. These hypergeometric functions have logarithmic divergency when $\xi/\xi_0 \to 1$. So the coefficients $C_\pm^{(\alpha)}$ and $C_\pm^{(\beta)}$ should counteract this divergency. Then we can get the retarded Green's functions in the outer IR region near $\xi \to 0$ as

$$\mathcal{G}_{\alpha\alpha}(\tilde{T}) = (2\pi\tilde{T})^{\delta_\alpha}\frac{\Gamma(\frac{3}{4} + \frac{\delta_\alpha}{4})\Gamma(\frac{1}{4} + \frac{\delta_\alpha}{4})\Gamma(1 - \frac{\delta_\alpha}{2})}{\Gamma(\frac{3}{4} - \frac{\delta_\alpha}{4})\Gamma(\frac{1}{4} - \frac{\delta_\alpha}{4})\Gamma(1 + \frac{\delta_\alpha}{2})},$$

$$\mathcal{G}_{\beta\beta}(\tilde{T}) = (2\pi\tilde{T})^{\delta_\beta}.$$

(48)

Now we can use the IR-UV matching method to express the UV Green's functions. Similar to the expression (40), we can get the Green's functions for α_1 and β_1 with some coefficients $a_\pm^{(n)}$ and $b_\pm^{(n)}$ which should be analytical functions of δB. Note that two retarded Green's functions have poles at $\delta B = T = 0$, we have,

$$G_{\alpha\alpha} = \frac{Z_1}{\delta B + c_1^{(\alpha)} T + \mathcal{G}_{\alpha\alpha}(T) c_2^{(\alpha)}},$$

$$G_{\beta\beta} = \frac{Z_2}{\delta B + c_1^{(\beta)} T + \mathcal{G}_{\beta\beta}(T) c_2^{(\beta)}}. \qquad (49)$$

Here $\mathcal{G}_{\alpha\alpha}$ is irrelevant and can be neglected. One should note $c_i^{(\beta)}$ are also the functions of $c_1^{(\alpha)}$ because the equation for β in the bulk depends on α but the equation for α in the bulk is independent on β. In the limit of $\delta B = 0$, we will find $\delta_\beta = 1$, so the $c_1^{(\beta)}$ term and $c_2^{(\beta)}$ term degenerate. In that case, as the case pointed out in Ref. [33], a logarithmic term appears. And the relevant terms in Green's functions read

$$G_{\alpha\alpha} = \frac{Z_1}{\delta B + c_1^{(\alpha)} T}, \qquad G_{\beta\beta} = \frac{Z_2}{\delta B + c_3^{(\beta)}(c_1^{(\alpha)}) T \ln T} \qquad (50)$$

with two constants Z_1 and Z_2. The poles for them are defined by,

$$\delta B + c_1^{(\alpha)} T = 0, \qquad \delta B + c_3^{(\beta)}(c_1^{(\alpha)}) T \ln T = 0. \quad (51)$$

Now note the fact that $\delta B \to -\delta B, c_1^{(\alpha)} \to -c_1^{(\alpha)}$ will lead $\alpha \to -\alpha$, which will not affect the solution of β, $c_3^{(\beta)}$ must be a function of $c_1^{(\alpha)2}$. Then in the case of $T \to 0$ and $\delta B \to 0$, there is a self-consistent ansatz such as $c_3^{(\beta)} = d_1 c_1^{(\alpha)2} + O(c_1^{(\alpha)4})$ for small $c_1^{(\alpha)2}$ and finite constant d_1.[2] Then we can see that the relevant parts of Eqs. (51) can be expressed as

$$\delta B + c_1^{(\alpha)} T = 0, \qquad \delta B + d_1 c_1^{(\alpha)2} T \ln T = 0. \qquad (52)$$

Solving these equations, we find $\delta B \propto T / \ln T$. As a result we have $b \equiv \delta B / B_c \propto T / \ln T$ and analytically show the relation (23).

D. Energy gap and correlation length in the quantum disordered phase

In Ref. [28], numerical results show that there is a gapped antiferromagnetic excitation in the quantum disordered phase. The energy gap and correlation length still obey the power law form (1c) and (1b) with respect to the tuning parameter b in the vicinity of QPT. These results can also be understood from the point of view of the emergent AdS$_2$ geometry.

---

[2] In general, the expansion of $c_3^{(\beta)}$ at small $c_1^{(\alpha)2}$ has a constant term such that d_0. This constant term must be zero; otherwise, equations (51) will not have solution if $\delta B \neq 0$.

In order to compute the energy gap of the antiferromagnetic excitation, we should turn on a perturbation for β with frequency ω. In the region of quantum disordered phase with $T = 0$ and $\delta B = B - B_c \to 0^+$, using the results in the previous section, the background and perturbation equations for polarization fields read

$$\alpha'' + \frac{f'\alpha'}{f} - \frac{m_{\alpha\text{eff}}^2}{r^2 f} \alpha - \frac{B}{r^2 f} = 0,$$

$$\tilde{\beta}'' + \frac{f'\tilde{\beta}'}{f} + \left[\frac{\omega^2}{r^2 f^2} - \frac{m_{\beta\text{eff}}^2}{r^2 f} \right] \tilde{\beta} = 0, \qquad (53)$$

and $\beta = 0$. The real frequency ω giving the pole for Green's function $G_{\beta\beta}(B)$ leads to the gapped quasi-particle excitation. To compute this Green's function, we take a similar method as in the previous subsections. In the IR region, considering the AdS$_2$ scaling limit at zero temperature, Eq. (53) can be written as

$$\frac{d^2\alpha}{d\xi^2} - \frac{B_c + \delta B + m_{\alpha\text{eff}}^2 \alpha}{6\xi^2} = 0, \qquad (54a)$$

$$\frac{d^2\tilde{\beta}}{d\xi^2} + \left(\tilde{\omega}^2 - \frac{m_{\beta\text{eff}}^2}{6\xi^2} \right) \tilde{\beta} = 0. \qquad (54b)$$

Up to the linear order of δB, Eq. (54a) gives the following regular solution with the IR fixed point:

$$\alpha = \alpha_c + \delta\alpha. \qquad (55)$$

Here $\delta\alpha$ is defined as (45). The equation for $\tilde{\beta}$ can be written as

$$\frac{d^2\tilde{\beta}}{d\xi^2} + \left[\tilde{\omega}^2 - \left(\frac{\partial m_{\beta\text{eff}}^2}{\partial\alpha} \right)_{\alpha=\alpha_c} \frac{\delta\alpha}{6\xi^2} \right] \tilde{\beta} = 0. \qquad (56)$$

Comparing it with Eq. (37) in subsection III B and noting the relationship in (45), one can easily find that the Green's function for $\tilde{\beta}$ has the following form,

$$G_{\beta\beta}(\omega) = \frac{Z_3}{-\delta B + e_1 \omega}, \qquad (57)$$

for small frequency ω and $\delta B \to 0^+$ with two nonzero constants e_1 and Z_3. Thus, we obtain the relation between the energy gap Δ and the magnetic field B as

$$\Delta \propto B - B_c, \qquad (58)$$

As to correlation length, it can be computed in a similar way by setting $\omega = 0$ but turning on the perturbation for β with nonzero moment q. In that case, we still have Eq. (54a), but Eq. (54b) is changed to

$$\frac{d^2\tilde{\beta}}{d\xi^2} - \frac{Q_0 q^2 + m_{\beta\text{eff}}^2}{6\xi^2} = 0. \qquad (59)$$

For small q and δB, it gives the Green's function as

$$G_{\beta\beta}(\omega) = \frac{Z_4}{q^2 + e_2 \delta B} = \frac{Z_4}{q^2 + 1/\xi^2}, \qquad (60)$$

where Z_4 is another constant and ξ is the correlation length. We then easily obtain

$$\xi \propto (B - B_c)^{-1/2}, \qquad (61)$$

which is the same as Eq. (1b) with $\nu = 1/2$.

We see that results (61) and (59) obey the universal scaling relations (1b) for quantum criticality with $z = 2$, i.e., $\Delta \propto |B - B_c|^{z\nu}$. This can be viewed as the self-consistency check for our model and computations.

IV. CONCLUSIONS AND DISCUSSIONS

A. Summarize the holographic model

We have investigated the quantum phase transition (QPT) from the antiferromagnetic phase (AF) to the quantum disordered phase (QD) and the criticality in the vicinity of the quantum critical point (QCP) in the antiferromagnetic materials induced by the magnetic field in a holographic model proposed in Ref. [26]. In the model, the Néel temperature T_N is suppressed by the magnetic field B. We have proved that there is a critical magnetic field B_c, at which $T_N = 0$ and a QPT occurs. In order to analytically study the critical behavior in the vicinity of QCP, we employed the IR-UV matching method in Ref. [33], and the results show that the analytical method confirms the numerical results obtained in Ref. [28]. In particular, we found that the dynamic exponent $z = 2$, which means that the boundary critical theory is indeed a strong coupling theory with effective dimension $d_{\text{eff}} = d + z = 4$. As a result, the hyperscaling law is violated and logarithmic corrections appear near the QCP. An interesting observation is that the critical behavior of the QCP is governed by the AdS_2 geometry emerging in the IR region of the background geometry.

B. Compare the results with RG flow

In this subsection, we will review the results from the field theory and compare them with the results from the holographic model. Our discussion on the field theory follows Ref. [6], and the details can be found there. A similar discussion to ours, but mainly for the case of $d = z = 2$, can be found in Ref. [34].

In the original work by Hertz to quantum criticality [2], he considered the coupling between fermions and the low-energy bosonic field which condenses at the QCP. By integrating the fast fermions, the effective field theory is the Landau-Ginsburg-Wilson (LGW) ϕ^4 theory with the upper critical dimension $d_c = 4 - z$, where z is the dynamical exponent. Near the QCP, we can get the

perturbative RG [35]. Here u, T_N, λ and b are the coupling constant, condensed temperature for bosonic field, scaling parameter and tuning parameter (in this paper, it is defined as $b = (B - B_c)/B$), respectively. Then the infinitesimal RG transformations are given by [35]

$$\frac{d\mathcal{T}}{d\ln\lambda} = z\mathcal{T}, \qquad (62a)$$

$$\frac{db}{d\ln\lambda} = 2b + uf_1(\mathcal{T}, b), \qquad (62b)$$

$$\frac{du}{d\ln\lambda} = (4 - d - z)u - u^2 f_2(\mathcal{T}, b), \qquad (62c)$$

with initial values $\mathcal{T} = T_N, b = b_0, u = u_0$. Here $f_1(\mathcal{T}, b)$ and $f_2(\mathcal{T}, b)$ are two functions of $\mathcal{T}, b$ defined by the details of the model. At low T close to the critical point $b = 0$, $f_1(T, b)$ can be expressed as the power series of T_N^2, and $f_2(\mathcal{T}, b)$ is constant. Thus, we can set $f_1(\mathcal{T}, b) = A_0 + A_1 T_N^2$ and $f_2(\mathcal{T}, b) = f_2$. The RG equations (62) have a Gaussian fixed point at $\mathcal{T} = u = b = 0$, which is unstable with respect to the tuning parameter b, so a phase transition may occur at this point (see Fig. 5). Since the RG equations are obtained by perturbations, we assume that the initial values satisfy $T_N, |b_0|, |u_0| \ll 1$. One of remarkable features is that this RG equation has a critical dimension at $d_c = d + z = 4$. So, in general, when $d > 4 - z$, we can find that the boundary of the ordered phase T_N (such as the AF transition temperature; see Fig. 1), energy scale Δ in the quantum disordered phase and the correlation length l in the vicinity of QCP obey the following scaling relations,

$$T_N \sim (-b)^\psi, \qquad \Delta \sim b^{\nu z}, \qquad l \sim b^{-\nu}, \qquad (63)$$

with $\psi = z/(d + z - 2)$, $\nu = 1/2$. However, this simple power law will lose its efficacy in the case of $d = z = 2$,
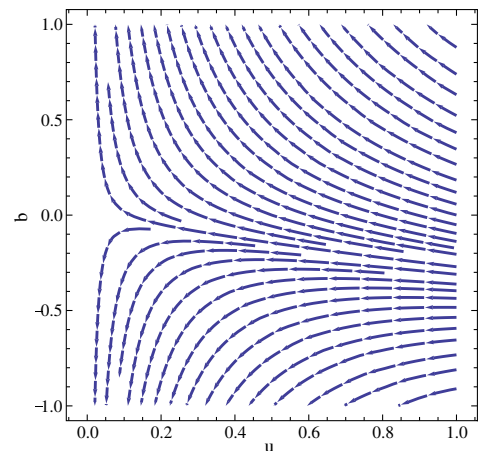

FIG. 5 (color online).   The schematic RG-flow diagram of $u - b$ for $d + z \geq 4$. There is a Gaussian fixed point at $u = b = 0$.

where the RG equations (62) need special consideration. In fact, the logarithmic correction on T_N appears. In order to see this, we directly solve $\mathcal{T}$, u from the RG equation (62a),

$$\mathcal{T}(\lambda) = T_N \lambda^z, \qquad u(\lambda) = \frac{u_0}{1 + u_0 A_2 \ln \lambda}. \qquad (64)$$

Next, integrating the scaling Eq. (62b) for $b(\lambda)$ and using Eqs. (62a) and (64), we find

$$b(\lambda) = \lambda^2 \left[b_0 + 2e^{\frac{2}{u_0 f_2}} E_1 \left(2 \ln \lambda + \frac{2}{u_0 f_2} \right) / (u_0 f_2) \right]. \quad (65)$$

Here $E_1(x)$ is the exponential integral function. For large real x, $E_1(x) \sim e^{-x}/x$. In the quantum critical region, using the scaling up to $\lambda \sim T_N^{-1/2}$, where $\mathcal{T} \sim 1$, we have

$$b(\lambda) = \frac{b_0}{T_N} + \frac{1}{f_2 u_0 \ln(1/T_N)} + O\left(\frac{1}{T \ln T} \right). \qquad (66)$$

Thus, we see that the scaling relation depends on the value of $b(\lambda)$ as $\lambda \to \infty$. However, the concrete form of $b(\lambda)$ cannot be found from the perturbational RG equations directly. Because of the strong-coupling feature in the case of $z = d = 2$, the perturbational methods cannot give complete information on the system. We see that the perturbation method fails in this case to give a complete result. If $b(\lambda)$ is a finite constant, then we can find a linear relation $b_0 \sim T_N$, which is just the usual power law. If $b(\lambda) \ln \lambda \to 0$ as $\lambda = 1/\sqrt{T_N} \to \infty$, then we can get $b_0 \sim T_N / \ln T_N$. Comparing with the usual power law, there is an additional logarithmic correction, the same as what we have obtained in the holographic model.

We see that, with some additional assumptions, the perturbational RG equations give the same results as the holographic model. In fact, in the case of $d = z = 2$, the low-energy Fermi liquid leads to long-range order-parameter interaction. As a result, the coefficients of the high-order interactions in the LGW functional diverge, leading to an infinite number marginal operators [31]. We see that the perturbational field method in this case fails to reveal a complete description. However, the holographic setup can give self-consistent and complete predictions.

C. Apply to real materials

Now let us turn our attention to real materials, whose properties might be described by the holographic model. The first candidate is what we call the magnetic pyrochlore oxides. They are characterized by the general chemical formula $A_2B_2O_7$, where A and B are various f- and d-elemental atoms, respectively.

Specifically, we focus here on the $Er_2Ti_2O_7$ and its various doped versions such as $Er_{2-2x}Y_{2x}Ti_2O_7$, where the parameter x describes the material in which the x-fraction of atoms Er is replaced by atoms Y. The Y atoms are usually located at arbitrary erbium replaced places, randomly distributed around the whole crystal. We consider only the cases where the value x is small ($x < 0.1$).

The magnetism in these compounds is associated with Er^{3+} ions. In the ground state of Er^{3+} ion the electron shell configuration is $4f^{11}6s^0$, that gives rise large total spin $J = 15/2$ which is associated with $L = 6$ and $S = 3/2$. It has a relatively moderate g-factor. The Lande factor is $g_J = 6/5$. The local crystal field (CF) of a trigonal D_{3d} point symmetry at the erbium sites splits the 16-fold degenerate state into eight doublets. Considering the sum of all these spin doublets associated with the single ion as a single total spin we note that these total spins are ordered in noncoplanar structure on the vertex-sharing tetrahedra [36,37]. The compound has a strong local XY-type anisotropy of magnetic moments arising due to the large orbital momentum of Er^{3+} ions, $L = 6$. Note that the anisotropy is not quenched by the crystal field and, therefore, there were suggestions to describe it with the use of 3D XY model [38]. The total spin of each tetrahedra is vanishing but may appear when magnetic field is applied or with doping x.

The detailed measurements of the low-temperature magnetic properties of compound and the analysis of these experimental data leads to the conclusion that the ground state is characterized by exotic spin dynamics [36,37], which is vanishing at the Néel's temperature, $T_N = 1.2$ K, via a second-order phase transition. There the co-existence of both the short- and long-range orders has been suggested. The Curie-Weiss temperature in $Er_2Ti_2O_7$ obtained from the susceptibility data, $\Theta_{CW} = 22K$, is significantly larger than T_N. The large ratio $\Theta_{CW}/T_N \approx 18 \gg 1$ indicates the existence of strong magnetic frustrations in the systems. To understand the role of magnetic frustrations in establishing long-range order is now one of the main challenges of condensed matter physics. They play probably an important role in the formation of the nontrivial antiferromagnetic non-coplanar structure observed [36,37].

The studies of $Er_2Ti_2O_7$ by heat-capacity measurements and electron-spin resonance spectroscopy performed on single-crystal samples allowed already to establish the consistent magnetic phase diagrams for two directions of applied field, H parallel to local [100] axes and H parallel to local [111] axes. [36]. In spite on the crystal anisotropy both phase diagrams are similar to each other. Muon spin relaxation measurements show the presence of spin dynamics in the nanosecond time scale down to 21 mK, that also illustrates the long- and short-range magnetic order, and the time scale not typical of conventional magnets [37]. Therefore, we will be interested to test the predictions of our holographic model to describe such exotic AF state, which is difficult to characterize by any other and conventional means. However, to address the question what we

can learn from the application of the holographic duality to these complex condensed matter systems, we have to look into the details of experimental data and the crystal and electronic structure they provide.

The magnetic excitation spectrum obtained with ESR [36] consists of a Goldstone mode, which has an isotropic gap in an applied field. When the magnetic field increases, there arises a field-induced quantum phase transition. This is possibly a second-order phase transition. It takes place at a critical field H_c above which the magnetization process is accompanied by a canting of the magnetic moments off their local easy planes [36].

One may notice that each tetrahedra, which has no net magnetic moment at $B = 0$ [36], has a quadruple moment. Therefore, for the ground state it would be natural to introduce the quadruple order parameter $Q_{\alpha\beta}$, e.g., associated with the spin structure of the individual tetrahedra. The antisymmetric part of this tensor can also describe a conventional magnetic moment or the dipole order parameter. Then the ground state may be described by the conventional Ginzburg-Landau (GL) expansion of the form

$$F = \alpha_0 Q_{\alpha\beta} Q^{\alpha\beta} + \beta_0 (Q_{\alpha\beta} Q^{\alpha\beta})^2 + \gamma_0 (Q_{\alpha\beta} F^{\alpha\beta}) + \cdots, \tag{67}$$

where α_0, β_0 and γ_0 are constants, the indices $\alpha(\beta) = x, y, z$, and the last term describes the interaction of the tetrahedron with the magnetic field. The minimization of the free energy with respect to $Q_{\alpha\beta}$ may provide the dependence of the order parameter on the temperature and the dependence of the critical temperature on the magnetic field of the form $T_c(H) = T_c(0) - cH^2$, where c is a constant.

In fact, for the real compound, $Er_2 Ti_2 O_7$, there are two types of tetrahedra having the different (opposite) orientations and forming two different sublattices. Similar to the classical antiferromagnet, each sublattice here will also have its own quadruple momentum. The sublattices may also have magnetic moments oppositely oriented, which are described by the antisymmetric part of the tensors. That is, we must have two order parameters, $Q_{\alpha\beta}^{(1)}$, and $Q_{\alpha\beta}^{(2)}$, and the GL expansion will now have three terms,

$$F = F_1 + F_2 + F_{12}, \tag{68}$$

where the functions F_1 and F_2 have the same form as Eq. (67), while the term F_{12} describes the interaction between these fields. One may already notice strong similarities between the GL expansion, F, and the Lagrangian of the holographic model, L. This similarity offers the suggestion that the polarization fields of the holographic model, $M^{(1)\mu\nu}$ and $M_{\mu\nu}^{(2)}$, play the same role as the quadruple fields used in the GL expansion, although

their spacial and matrix dimensions are different. Note that the analogous similarity also exists between the GL theory of superconductivity and the holographic superconductor model [21]. Thus, following this observation, we arrive at the remarkable conclusion that the holographic model describes an exotic magnetic state where the antiferromagnetic and quadruple ordering coexist.

Note that these two approaches, GL and holographic, are very different: one has an explicit dependence on temperature in its coefficients, while the other does not. In addition, the physical meanings of the parameters in the two approaches are different. In the AdS/CFT correspondence, if one knows the theories on both sides, we can connect the bulk parameters to the parameters in the boundary theory. Unfortunately, here we take the bottom-up approach, where the boundary theory is not yet available; thus, we are here not able to give a precise clear physical interpretation of the bulk parameters in terms of the boundary microscopic model. However, for the case of the ferromagnetics/paramagnetics phase transition [39], the connection between the parameters of the bulk and boundary theories has been made assuming that the boundary of the AdS space is described by a kind of Ising-like model.

Here, by considering this analogy between the GL expansion and the proposed holographic model, we are trying to give an intuitive interpretation of the physical meaning for the parameters of the holographic model. The parameter k/m^2 describes an effective interaction between the quadruple moments of two pyrochlore sublattices and, therefore, should be proportional to the exchange constants associated with the interaction between the spins in these tetrahedra, while the parameter J describes the value of the quadruple amplitude induced on individual tetrahedra. It should be inversely proportional to the exchange constants between the spins associated with a single individual tetrahedron. Therefore, when the modulus J increases, we expect to have ordered states such as ferro-, ferri-, or antiferromagnetic ones, with the latter depending on the relation between J and k/m^2. Also, when k is positive we expect to have AF ordering, but when it is negative, the ordering with nonvanishing magnetic moment may arise. Indeed, these arguments are in qualitative agreement with the precise phase diagram of different possible states which can be obtained with the use of the proposed holographic model; see Fig. 2. In this figure we also see that the holographic model predicts the existence of the ferrimagnetic phase in the large region of the phase diagram existing even when the parameter k/m^2 is positive while J is negative. The phase boundary is described by the equation

$$J \approx -1.2(k - m^2)^2 / 4m^4. \tag{69}$$

This is a very remarkable result, which also indicates that the holographic model can be applied to other complex pyrochlore materials having magnetic frustration which are

leading to the formation of complex magnetic phases such as those observed at the spin glass freezing in $Y_2Mo_2O_7$, in spin ice in $Ho_2Ti_2O_7$, $Dy_2Ti_2O_7$ and $Tb_2Sn_2O_7$, at the anomalous spin Hall effect in $Nd_2Mo_2O_7$, and in the Kondo effect in $Pr_2Ir_2O_7$ [40]. The holographic model can also describe the ferrimagnetic phases in other compounds having complex magnetic structure, such as those observed in recently synthesized Pd-based ternary compounds of the form R_2PdSi_3, where R is a rare earth atom (see Ref. [41]). There, e.g. in Tb_2PdSi_3, the interplay of the complex structure and magnetic frustrations leads to the formation of the clustered ferrimagnetic phase [41].

It is also interesting to make a comparison with existing theories of the magnetic states and phase transitions in $Er_2Ti_2O_7$. From the first glance, the behavior of this compound should be very complex because the nearest neighbor exchange, the Dzyaloshinskii-Moriya, the dipolar, and the magnetoelastic interactions do exist. They all play an important role in the formation of the low-temperature frustrated antiferromagnetic state. Therefore, it is a real challenge to develop an adequate theory here. In spite of this fact, the theory made a few advances. It was suggested that due to strong frustrations, the ordering state in this compound is formed by quantum disorder, i.e., in a very unconventional way [13]. In another approach, a three-dimensional XY-like theoretical model has been proposed in [38]. The key role in the model is played by the isotropic exchange between transverse components of nearest-neighbor spins and bond-dependent exchange anisotropy. There, local spins are coupled by nearest-neighbor anti-ferromagnetic exchange interaction.

Due to the large spins the long-range dipole-dipole interactions on the pyrochlore lattice do exist, too, but to take this into account leads to significant technical diffi-culties. However, Zhitomirsky *et al.* have shown [38] that the interplay of these multiple interactions with the existing frustrations dictates indeed the formation of the antiferro-magnetic ground state and there the quantum disorder mechanism is playing a key role. The inclusion of the exchange anisotropy only reproduces the well observed second-order magnetic phase transition in $Er_2Ti_2O_7$ at zero field. However, when magnetic field increases some chal-lenges associated with the frustration on the pyrochlore lattice arise. To address the issue, Oitmaa *et al.* [42] have argued that the dipolar interactions make also an important contribution into the formation of the AF state and into the second order phase transition observed [13].

Probably as it was argued in Ref. [38] the exchange and anisotropy interactions may overcome the dipolar inter-action at zero magnetic field where the tetrahedral magnetic units have no net magnetic moment in the ground state, but this is not the case when the magnetic field is on. Then the dipole-dipole interaction and frustrations existing on the pyrochlore lattice become very important and can not be neglected. Therefore, so far the field evolution of the

antiferromagnetic state and the role of the long-range part of the dipole-dipole interactions and magnetic frustrations in such an evolution remained a puzzling issue and were beyond the scope of the discussed models. To address these issues here we proposed a holographic model which effectively absorbs all existing interactions in $Er_2Ti_2O_7$ in a form of strongly interacting tensor or quadrupole-like fields embedded in AdS space of a higher dimension.

The extra dimension of the AdS space plays a role of the renormalization parameter, which separates relevant and irrelevant degrees of freedom in the system. The proposed holographic model describes well not only the zero-temperature thermodynamic phase transition and spin wave excitation spectrum observed in $Er_2Ti_2O_7$ but also their evolution in the applied magnetic field [28]. The model allows also to uncover an intriguing picture of many possible coexisting phases, which can arise at such a complexity of interactions existing in $Er_2Ti_2O_7$ [43]. For this purpose to uncover the possible correlations associated with the deformation of the AF state observed we have to calculate and investigate various correlation functions in magnetic field. To find these correlation functions will be reduced to the solution of different PDE equations. It is viable, although very time consuming, work. The power of the holographic model provides this opportunity never existed before

In particular, in Ref. [43] it was experimentally found that with magnetic order there exist well-defined spin wave excitations. With the applied magnetic field, their spectrum is softening (see the spin wave spectrum measured at the field 1.5 T on Fig. 4 in Ref. [43]). This behavior is in perfect agreement with the prediction of the holographic model. In the studies of an array of magnetic particles where the dipolar interaction is usually relevant, it was shown that its long-range character may lead to a formation of a landscape of low-energy states [44,45]. With increasing field, the spins form canted states and the energy landscape is flattening. There may arise continuous switching between these states. Therefore, such an evolution in magnetic field may lead to a quantum critical behavior and an appearance of quantum critical point (QCP) as described here by the holographic model. Indeed, the analysis of the low-temperature phase diagram of $Er_2Ti_2O_7$ made in Ref. [43] supports the existence of the rich variety of elementary excitations, as the ground state is tuned by an external magnetic field. The authors of Ref. [43] also suggested that most dramatic variations of the spectra with field arising at 1.5 T may possibly correspond to the formation of a continuous QCP. Indeed, in the framework of our holographic model a similar picture emerges: the magnetic AF order continuously changes with the field until the QCP arises. The holographic model predicts the precise value of the critical field, $B_c \simeq 1.45$ T, for the QCP.

The holographic model provides not only qualitative but also quantitative description of the experimental
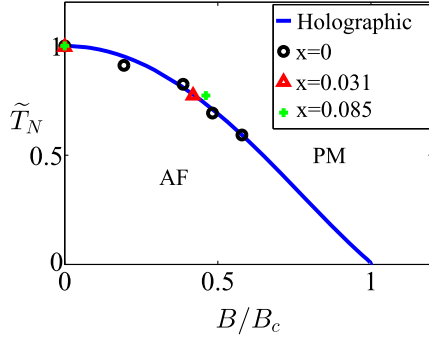
FIG. 6 (color online). The antiferromagnetic critical temperature T_N versus the external magnetic field B calculated at the best fitting model parameters $m^2 = 1, k = 7/8$ and $J = -0.71$ (solid curve) and compared with experimental data for pyrochlore compounds, $Er_{2-2x}Y_{2x}Ti_2O_7$ with three different doping x. Black circles corresponds to zero doping, $x = 0$; magenta triangulars—to $x = 0.031$; green crosses—to $x = 0.085$. The experimental data are from [13] and the figure is from [28].

data [12,13] of the Néel temperature lowering with magnetic field (see Fig. 6) and predicts the QCP at 1.45T, which is very close to the value which can be deduced from the extrapolation of the experimental results to the critical region of the field. More experiments are needed to investigate the critical region in detail and to verify all predictions of the model described in this paper. Of course, we should mention here that the good fitting of the existing experimental data by the holographic theory only shows its usefulness.

We find that similar quantum critical point and analogous behavior in the magnetic field exists for other pyrochlore compounds such as $Er_{2-2x}Y_{2x}Ti_2O_7$ obtained from parent $Er_2Ti_2O_7$ compound by Y^{3+} doping. Note that the Y^{3+}-ion has no magnetic moment and, therefore, doping removes magnetic moments from the pyrochlore structure. This breaks the balance of magnetic ordering on individual tetrahedra, increases frustrations and reduces naturally an effective interaction between magnetic moments in the compound. Thus, according to the physical intuition, the Néel temperature should decrease. Experiments reveal a very remarkable fact that both doping and the increasing of magnetic field decrease the Néel temperature of the Y^{3+}-doped and undoped $Er_2Ti_2O_7$ compounds in a very similar fashion. This fact is very difficult to explain in a framework of any existing so far microscopic model. However this fact is in complete agreement with the predictions of the holographic model, which shows that the doping by the nonmagnetic Y^{3+} ions decreases the quadruple (or polarisation) fields in a very similar fashion as the external magnetic field does and, therefore, all these doped systems and their spectrum of elementary excitations behave in the magnetic field very similarly and so the QCP should arise (see Fig. 6).

For an illustration on this figure, the Néel temperature of the Y^{3+}-doped compound is rescaled to the critical

temperature of the undoped one. We see from this figure that the rescaled critical temperature dependence on the critical magnetic field is a universal function and is independent on the nonmagnetic doping at the magnetic sites. This fact that the influence of dilution in $(Er_{1-x}Y_x)_2Ti_2O_7$ solid solutions is similar to the increase of the magnetic field for pure $Er_2Ti_2O_7$ stresses once more the importance of strong correlations, strong coupling and the universality of complex magnetic interactions in these systems which can be well described in the framework of the proposed holographic approach. Indeed, as expected, holographic theories give some universal properties of a class of materials.

In addition, we see that the high-field ground state does not correspond to a simple disordered paramagnet. At the QCP, magnetic spins become partially aligned in the direction of the magnetic field. Therefore, the system requires less thermal energy to destroy the remaining magnetic spins order. We see that high-field state where the magnetic field is higher than the critical field is characterized by the intense dispersive excitation, whose dispersion increases with the field. This prediction of the holographic model is in agreement with the recent observations of elementary excitations in $Er_{2-2x}Y_{2x}Ti_2O_7$ reported in Ref. [43]. There it was found that the critical fluctuations of the low-field AF state are accompanied by a precursor of the intense dispersive excitation noticed at the high field only.

In Fig. 7, we show the magnetic energy gap of $Er_{2-2x}Y_{2x}Ti_2O_7$ as a function of magnetic dilution (x) and magnetic field [13]. One should note that, in Fig. 4 of Ref. [43], the excitation energy gap of the undoped compound is zero, when $B < B_c$ and $T \to 0$. But in the doped compound a nonzero energy gap ($\simeq 0.18$ meV) has been noticed even when the magnetic field is smaller than
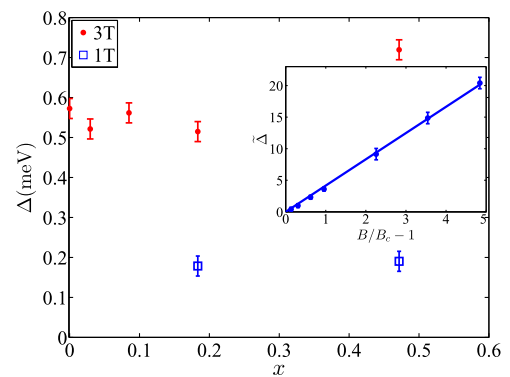

FIG. 7 (color online). The energy gap of the high-field ferrimagnetic state, Δ, of $Er_{2-2x}Y_{2x}Ti_2O_7$ as a function of magnetic dilution (x) and magnetic field B measured in the units of the critical field. The data are taken from Ref. [13]. The insert shows the energy gap with respective to magnetic field when $x = 0$, where the solid line represents the best theoretical fitting curve.

the critical one, $B < B_c$ (see the plotted data associated with $B = 1$ T presented by blue squares in Fig. 7). This gap has been detected by the magnetic heat capacity method (see, for details, Ref. [13]). The fact that in the AF state with the small doping there arises a gap indicates the formation of the droplets with a spin liquid. Such droplets are mostly induced by dopant impurities and formed in their vicinity. The appearance of such droplets is not significant to the destruction of the long-range order, which is associated with the AF state, since droplets with spin liquid have short-range correlations only.

Therefore, to extract the elementary excitations of the high-field state, the background associated with the creation of the magnetic inhomogeneities should be removed. After removing this background, we find the energy gap in the spectrum of elementary excitations [13]. This experimentally found dependence of the gap on the magnetic field just satisfies the linear relation (58). This is exactly the relation derived from the holographic model,

$$\tilde{\Delta} \propto B/B_c - 1, \tag{70}$$

with $\tilde{\Delta} = \Delta/T_N$.

In the inset of Fig. 7 we plot the experimental data and the fitting curve by Eq. (70). Note that, in principle, the relation (70) holds only near the critical point from the holographic model. However, we see that the linear relation fits the experimental data very well even for a large derivation from the critical point. The slope of the fitting curve is 4.2. We can also obtain this slope from the holographic approach under the parameters with the best fitting we used in Fig. 6, which gives the slope 5.0. So we see that our holographic model can not only fit well the $T_N - B$ behavior but also predict the QCP and associated critical magnetic field. This prediction gives the exact value deduced from the extrapolation of the existing measurements to the critical region. The holographic model also predicts the existence of the novel ferrimagnetic phase arising in the field larger than the critical one. In this high-field phase, there appears a gap which linearly increases with the magnetic field with a constant slope. In the previous estimation of this slope, we considered the g factor for electrons in vacuum, where $g = 2$. Usually, in solids it is smaller than 2. However, a slight tuning of the parameter λ, which plays a role of the g factor in our model, will not change the equation of motion and the form of the phase diagram on the Fig. 6. However, it gives the precise value for the slope equal to 4.2. Therefore, with this tuning of λ, we get smaller value for the g factor and, therefore, we may get a perfect agreement with the experimental data.

We have also found that the holographic model describes well the magnetic properties of other classes of materials, which have strong magnetic anisotropy and large magnetic moments. The most illustrative example is $BiCoPO_5$ [12,28]. The compound consists of the interacting spins chains giving the quasi-one-dimensional character to the compound. The spins have large magnetic moments, about 5.2 μ_B per Co^{2+} ion measured at 1.5 K [12]. It is much higher than the value 3.9 μ_B expected for Co^{2+} ions having $S = 3/2$. Such a large value of μ_{eff} is rather typical in Co^{2+}-contained compounds due to the additional orbital magnetic moment in the oxygen octahedra existing around the Co^{2+} ions.

The magnetic structure can be determined with the powder neutron diffraction experiments [46]. It was suggested there that the ferromagnetic pairs of Co^{2+} ions are antiferromagnetically coupled within double chains. Because of these large values of the ferromagnetic pairs of Co^{2+} ions, there exists a dipole-dipole interaction between the resulting magnetic moments, which is probably significantly weaker than the exchange interactions. There is also a strong spin-orbital interaction, which always exists in heavy atoms such as Bi. The competition of all these interactions is probably responsible for the deviation from collinear AF ground state in $BiCoPO_5$ [46]. In this sense the situation is very similar to the case of pyrochlore materials discussed above in Fig. 6. Therefore, as in the above, the long-range large interacting moments here can be replaced by the interacting tensor fields. It was found that the magnetic anisotropy and arrangements of magnetic moments in $BiCoPO_5$ can be continuously tuned by temperature and external magnetic field [47].

However, neither field-induced order-disorder nor spin-flop transition was found in the susceptibility and specific heat measurements under the external field, although the spin-flop transition was seen in the magnetization dependence on the magnetic field measured at $T = 2$ K [12]. The Néel temperature, T_N, and AF order were found to decrease gradually with the increase of magnetic field. But even at high fields, no extra features other than the Néel transition were observed in the specific heat [12] until the AF order was completely suppressed. Such behavior is consistent with the prediction of our holographic model, suggesting that the quite strong and continuous change in magnetic anisotropy with the field may be well described with the interacting tensor fields embedded in the gravitational AdS space, i.e., with the aid of the AdS/CFT duality.

The holographic approach is very general and, therefore, it can also address very unusual magnetic properties in many compounds where antiferromagnetic ordering may coexist with ferromagnetic and exotic magnetic (e.g., ferrimagnetic) phases are established. One of these materials is the recently discovered Tb_2PdSi_3 compound [41]. There, some kind of long-range magnetic ordering sets in below the Néel temperature, $T_N = 23.6$ K. The magnetism appears there to be very complex (see Fig. 1 of the Ref. [41]), and neutron diffraction studies in the zero magnetic field revealed both the long- and short-range order; i.e., it is very similar to the properties of the magnetic pyrochlore $Er_{2-2x}Y_{2x}Ti_2O_7$ discussed in this section.

Therefore, our holographic model predicts that in Tb$_2$PdSi$_3$, there will arise a quantum phase transition when the magnetic field reaches a value $B_c = 28.3$ T and a formation of a new ferrimagnetic phase with gapfull excitations described by Eq. (70) in a stronger field.

[1] S. Sachdev and B. Keimer, Quantum criticality, Phys. Today **64**, 29 (2011).

[2] J. A. Hertz, Quantum critical phenomena, Phys. Rev. B **14**, 1165 (1976).

[3] S. Sachdev, *Quantum Phase Transitions* (Cambridge University Press, Cambridge, England, 1999).

[4] Focus issue: Quantum phase transitions, Nat. Phys. **4**, 167 (2008).

[5] P. Gegenwart, Q. Si, and F. Steglich, Quantum criticality in heavy-fermion metals, Nat. Phys. **4**, 186 (2008).

[6] H. v. Lohneysen, A. Rosch, M. Vojta, and P. Wolfle, Fermi-liquid instabilities at magnetic quantum phase transitions, Rev. Mod. Phys. **79**, 1015 (2007).

[7] Q. Si, S. Rabello, K. Ingersent, and J. L. Smith, Locally critical quantum phase transitions in strongly correlated metals, Nature (London) **413**, 804 (2001).

[8] T. Senthil, A. Vishwanath, L. Balents, S. Sachdev, and M. P. A. Fisher, Deconfined quantum critical points, Science **303**, 1490 (2004); H. Tanaka, A. Oosawa, T. Kato, H. Uekusa, Y. Ohashi, K. Kakurai, and A. Hoser, Observation of field-induced transverse Néel ordering in the spin gap system TlCuCl$_3$, J. Phys. Soc. Jpn. **70**, 939 (2001).

[9] G. Chaboussant, P. A. Crowell, L. P. Levy, O. Piovesana, A. Madouri, and D. Mailly, Experimental phase diagram of Cu$_2$(C$_5$H$_{12}$N$_2$)$_2$Cl$_4$: A quasi-one-dimensional antiferromagnetic spin-Heisenberg ladder, Phys. Rev. B **55**, 3046 (1997).

[10] W. Shiramura, K. Takatsu, H. Tanaka, K. Kamishima, M. Takahashi, H. Mitamura, and T. Goto, High-field magnetization processes of double spin chain systems KCuCl$_3$ and TlCuCl$_3$, J. Phys. Soc. Jpn. **66**, 1900 (1997); A. Oosawa, T. Takamasu, K. Tatani, H. Abe, N. Tsujii, O. Suzuki, H. Tanaka, G. Kido, and K. Kindo, Field-induced magnetic ordering in the quantum spin system KCuCl$_3$, Phys. Rev. B **66**, 104405 (2002).

[11] Ch. Rüegg, N. Cavadini, A. Furrer, H.-U. Gdel, K. Krämer, H. Mutka, A. Wildes, K. Habicht, and P. Vorderwisch, Bose-Einstein condensation of the triplet states in the magnetic insulator TlCuCl$_3$, Nature (London) **423**, 62 (2003); T. Nikuni, M. Oshikawa, A. Oosawa, and H. Tanaka, Bose-Einstein Condensation of Dilute Magnons in TlCuCl$_3$, Phys. Rev. Lett. **84**, 5868 (2000).

[12] E. Mathews, K. M. Ranjith, M. Baenitz, and R. Nath, Field induced magnetic transition in low-dimensional magnets Bi(Ni, Co)PO$_5$, Solid State Commun. **154**, 56 (2013).

[13] J. F. Niven, M. B. Johnson, A. Bourque, P. J. Murray, D. D. James, H. A. Dabkowska, B. D. Gaulin, and M. A. White, Magnetic phase transitions and magnetic entropy in the XY antiferromagnetic pyrochlores(Er$_{1-x}$Y$_x$)$_2$Ti$_2$O$_7$, Proc. R. Soc. A **470**, 20140387 (2014).

[14] Ch. Rüegg, B. Normand, M. Matsumoto, A. Furrer, D. F. McMorrow, K. W. Krämer, H.-U. Güdel, S. N. Gvasaliya, H. Mutka, and M. Boehm, Quantum Magnets under Pressure: Controlling Elementary Excitations in TlCuCl$_3$, Phys. Rev. Lett. **100**, 205701 (2008).

[15] J. M. Maldacena, The large N limit of superconformal field theories and supergravity, Adv. Theor. Math. Phys. **2**, 231 (1998); Int. J. Theor. Phys. **38**, 1113 (1999).

[16] S. S. Gubser, I. R. Klebanov, and A. M. Polyakov, Gauge theory correlators from non-critical string theory, Phys. Lett. B **428**, 105 (1998).

[17] E. Witten, Anti-de Sitter space and holography, Adv. Theor. Math. Phys. **2**, 253 (1998).

[18] E. Witten, Anti-de Sitter space, thermal phase transition, and confinement in gauge theories, Adv. Theor. Math. Phys. **2**, 505 (1998).

[19] S. S. Gubser, Breaking an Abelian gauge symmetry near a black hole horizon, Phys. Rev. D **78**, 065034 (2008).

[20] S. A. Hartnoll, C. P. Herzog, and G. T. Horowitz, Building a Holographic Superconductor, Phys. Rev. Lett. **101**, 031601 (2008).

[21] R. G. Cai, L. Li, L. F. Li, and R. Q. Yang, Introduction to holographic superconductor models, Sci. China Phys. Mech. Astron. **58**, 1 (2015).

[22] S.-S. Lee, A non-Fermi liquid from a charged black hole: A critical Fermi ball, Phys. Rev. D **79**, 086006 (2009).

[23] H. Liu, J. McGreevy, and D. Vegh, Non-Fermi liquids from holography, Phys. Rev. D **83**, 065029 (2011).

[24] M. Cubrovic, J. Zaanen, and K. Schalm, String theory, quantum phase transitions and the emergent Fermi-liquid, Science **325**, 439 (2009).

[25] R.-G. Cai and R.-Q. Yang, Paramagnetism-ferromagnetism phase transition in a dyonic black hole, Phys. Rev. D **90**, 081901 (2014).

[26] R. G. Cai and R. Q. Yang, Holographic model for the paramagnetism/antiferromagnetism phase transition, Phys. Rev. D **91**, 086001 (2015).

[27] R. G. Cai and R. Q. Yang, Antisymmetric tensor field and spontaneous magnetization in holographic duality, arXiv:1504.00855.

[28] R. G. Cai, R. Q. Yang, and F. V. Kusmartsev, A holographic model for antiferromagnetic quantum phase transition induced by magnetic field, arXiv:1501.04481.

[29] R.-G. Cai and Y.-Z. Zhang, Black plane solutions in four-dimensional space-times, Phys. Rev. D **54**, 4891 (1996).

[30] N. Iqbal, H. Liu, M. Mezei, and Q. Si, Quantum phase transitions in holographic models of magnetism and superconductors, Phys. Rev. D 82, 045002 (2010).

[31] Ar. Abanov and A. Chubukov, Anomalous Scaling at the Quantum Critical Point in Itinerant Antiferromagnets, Phys. Rev. Lett. 93, 255702 (2004).

[32] S. Sachdev and E. R. Dunkel, Quantum critical dynamics of the two-dimensional Bose gas, Phys. Rev. B 73, 085116 (2006).

[33] T. Faulkner, H. Liu, J. McGreevy, and D. Vegh, Emergent quantum criticality, Fermi surfaces, and AdS(2), Phys. Rev. D 83, 125002 (2011).

[34] J. Bauer, P. Jakubczyk, and W. Metzner, Critical temperature and Ginzburg region near a quantum critical point in two-dimensional metals, Phys. Rev. B 84, 075122 (2011).

[35] A. J. Millis, Effect of a nonzero temperature on quantum critical points in itinerant fermion systems, Phys. Rev. B 48, 7183 (1993).

[36] S. S. Sosin and L. A. Prozorova, M. R. Lees, G. Balakrishnan, and O. A. Petrenko, Magnetic excitations in the XY-pyrochlore antiferromagnet $Er_2Ti_2O_7$, Phys. Rev. B 82, 094428 (2010).

[37] P. Dalmas de Reotier, A. Yaouanc, Y. Chapuis, S. H. Curnoe, B. Grenier, E. Ressouche, C. Marin, J. Lago, C. Baines, and S. R. Giblin, Magnetic order, magnetic correlations, and spin dynamics in the pyrochlore antiferromagnet $Er_2Ti_2O_7$, Phys. Rev. B 86, 104424 (2012).

[38] M. E. Zhitomirsky, M. V. Gvozdikova, P. C. W. Holdsworth, and R. Moessner, Quantum Order by Disorder and Accidental Soft Mode in $Er_2Ti_2O_7$, Phys. Rev. Lett. 109, 077204 (2012).

[39] R. G. Cai, R. Q. Yang, Y. B. Wu, and C. Y. Zhang, Massive 2-form field and holographic ferromagnetic phase transition, arXiv:1507.00546.

[40] J. S. Gardner, M. J. P. Gingras, and J. E. Greedan, Magnetic pyrochlore oxides, Rev. Mod. Phys. 82, 53 (2010).

[41] N. N. Kovaleva, K. I. KugelA. V. Bazhenov, T. N. Fursova, W. Loeser, Y. Xu, G. Behr, and F. V. Kusmartsev, Formation of metallic magnetic clusters in a Kondo-lattice metal: Evidence from an optical study, Sci. Rep. 2, 890 (2012).

[42] J. Oitmaa, R. R. P. Singh, B. Javanparast, A. G. R. Day, B. V. Bagheri, and M. J. P. Gingras, Phase transition and thermal order-by-disorder in the pyrochlore antiferromagnetic $Er_2Ti_2O_7$: a high-temperature series expansion study, Phys. Rev. B 88, 220404 (2013).

[43] J. P. C. Ruff, J. P. Clancy, A. Bourque, M. A. White, M. Ramazanoglu, J. S. Gardner, Y. Qiu, J. R. D. Copley, M. B. Johnson, H. A. Dabkowska, and B. D. Gaulin, Spin Waves and Quantum Criticality in the Frustrated XY Pyrochlore Antiferromagnet $Er_2Ti_2O_7$, Phys. Rev. Lett. 101, 147205 (2008).

[44] D. M. Forrester, K. E. Kuerten, and F. V. Kusmartsev, Magnetic cellular automata and the formation of glassy and magnetic structures from a chain of magnetic particles, Phys. Rev. B 75, 014416 (2007).

[45] K. E. Kurten and F. V. Kusmartsev, Fractal structures in systems made of small magnetic particles, Phys. Rev. B 72, 014433 (2005).

[46] O. Mentre, F. Bouree, J. Rodriguez-Carvajal, A. El. Jazouli, N. El. Khayati, and El. M. Ketatni, "Magnetic structure and analysis of the exchange interactions in $BiMO(PO_4)$ (M = Co, Ni)," J. Phys. Condens. Matter, 20, 415211 (2008).

[47] H. Yamaguchi, S. Yasin, S. Zherlitsyn, K. Omura, S. Kimura, S. Yoshii, K. Okunishi, Z. He, T. Taniyama, M. Itoh, and M. Hagiwara, "Novel Phase Transition Probed by Sound Velocity in Quasi-One-Dimensional Ising-Like Antiferromagnet $BaCo_2V_2O_8$," J. Phys. Soc. Jpn., 80, 033701 (2011).